Holger J. Konle[1]
e-mail: holger.konle@pi.tu-berlin.de

Christian O. Paschereit
e-mail: oliver.paschereit@tu-berlin.de
Technische Universität Berlin,
Müller-Breslau-Strasse 8,
10623 Berlin, Germany

Ingo Röhle
German Aerospace Center,
Bunsenstrasse 10,
37073 Göttingen, Germany
e-mail: ingo.roehle@dlr.de

Application of Fiber-Optical Microphone for Thermo-Acoustic Measurements

A high temperature resistant fiber-optical microphone (FOM) was developed and successfully applied in a combustion chamber at a thermal power of 8.4 kW to measure thermo-acoustic oscillations at a frequency of 85 Hz and a sound pressure level of 154 dB. The sensor head temperature was estimated to ~1000 K. The core of the optical setup used for the FOM is a Fabry–Perot interferometer. To create an acoustical sensor based on this type of interferometer, a new method of generation and postprocessing of the interference signal was developed. The simple replaceability of the sensor membrane reduces the requirements concerning the sensor handling compared with conventional condenser microphones and allows the adaptation of the sensor sensitivity to its application case changing the membrane stiffness. [DOI: 10.1115/1.4001983]

1 Introduction

Design and development of new gas turbines focus mainly on the realization of combustion systems with low emissions concerning both pollutants and noise. Therefore, different combustor designs, which are based on lean premixed combustion, are currently under investigation. This type of combustion, however, is often accompanied by combustion instabilities increasing the emissions aimed to be reduced and resulting in lower setup performance or even in the break-down of the facility (see, e.g., Refs. [1–3]). To study the occurrence of such combustion oscillations, appropriate instrumentation to monitor the acoustics of the combustion facility has to be provided.

State-of-the-art measurement techniques for combustion driven acoustic pressure oscillations, however, show severe application limitations: Conventional condenser microphones cover a wide dynamic range and are very suitable for acoustic measurement but are restricted to temperatures below 150 °C and, therefore, an application at temperatures exceeding this limit is not possible without special efforts. References [4–6] show the possibility to apply condenser microphones wall flush-mounted even at higher temperatures using water-cooled holders for the sensors. However, all water-cooled sensors require a constant (or at least controlled) water temperature to stabilize the sensor sensitivity while being accompanied by their highly increased space requirement.

Piezoelectric and piezoresistive pressure transducers with high temperature and/or high pressure resistant designs are commercially available but the dynamic ranges of these sensor types are limited. Models, which cover the dynamic range of interest concerning thermo-acoustic experiments, require again special cooling systems accompanied by the same drawbacks as condenser microphones. Reference [7] presents, e.g., a highly complex design of a sensor housing based on water cooling enabling pressure oscillation measurements with piezoresistive sensors at temperatures up to 1100–1400 K.

Special sensor designs, called probe sensors or remoting system based sensors, which are generally based on one of the aforementioned techniques, enable the high temperature and high pressure measurement while separating the position of the sensitive sensor from the position where the acoustic pressure of interest has to be measured. Therefore, generally, at least a tube is used for transmitting the acoustic signal to the sensor. This tube, however, increases the stiffness of the sensor setup and its transfer function has to be taken into account processing the sensor data (see, e.g., Refs. [8–11]). The accordant transfer function is not only often modeled with a number of necessary simplifications but it can also be obtained experimentally by means of special and complex calibration setups. More information on this experimental determination of the transfer function and the application of probe microphones can be found, e.g., in Refs. [12–16].

Several probe designs have been proposed in these references including different ways to cool the sensors and to prevent hot gases from entering the tube. In consequence, the consideration of the influence of the resulting temperature gradient on the transfer function of the tube has also been postulated [17].

A new measurement technique with a high potential to cover the field of acoustic measurements in harsh environments, while requiring neither special cooling nor increased space, is the technique of fiber-optical microphones. Different extrinsic fiber designs are possible. The presented paper describes a prototype based on the interferometric detection of acoustically induced membrane displacements. To enable its application in harsh environments, a highly stable optical setup has been designed and used to realize this first fiber-optical microphone (FOM) prototype.

In general, fiber-optical sensors combine the following advantages.

- The sensors can be constructed of high temperature resistant materials.
- The sensor is immune to electromagnetic interference and radio-frequency interference.
- The sensor has a high capability to be miniaturized.

The following section presents the basic idea to set up an FOM and states the disadvantages of commercial interferometers that have been tested in the past to create an FOM [18,19]. Afterward, the interferometer used to set up the first prototype for combustion diagnostics is introduced. The subsequent part presents results of experiments performed under cold and hot conditions. Finally, the current application limitations are clarified and suggestions for further improvements of the technique are presented.

[1]Corresponding author.

Contributed by the International Gas Turbine Institute (IGTI) of ASME for publication in the JOURNAL OF ENGINEERING FOR GAS TURBINES AND POWER. Manuscript received April 8, 2010; final manuscript received April 8, 2010; published online September 14, 2010. Editor: Dilip R. Ballal.

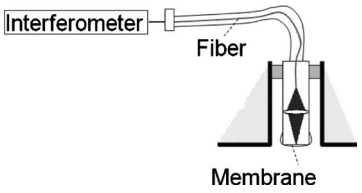

Fig. 1 Principle setup of an extrinsic, fiber based FOM

2 Setup of a Fiber-Optical Microphone Based on Interferometry

Figure 1 shows the principle setup of a FOM based on the interferometric detection of acoustically induced membrane movements. A laser beam is guided via a glass fiber to the back of a reflecting membrane on which the measurement beam is focused by means of a lens. The reflection of the beam is collected via the same lens and coupled back into the fiber. The projection of the collected beam reflection and its accordant reference beam on a photo receiver (e.g., an avalanche diode or PIN diode) enables the monitoring of the resulting interference signal. The movement of the membrane induced by the acoustic field that has to be measured influences the phase of the two interfering beams and, thus, the acquired interference signal correlates to the acoustic signal. To build up a stable FOM prototype, which is both high temperature resistant and insensitive to fiber vibrations, the use of an interferometric setup is needed, which fulfills the two following requirements.

- The setup can be based on nonpolarization maintaining singlemode fibers with special metal coatings, which enable application temperatures in the range of 800–1000 K.
- The two interfering beams are both traveling the glass fiber, thus, fiber vibrations have no influence on the relative phase between the interfering beams.

These requirements can be met with a fiber based Fabry–Perot interferometer. This interferometer type is created automatically by the cavity between the end of a singlemode glass fiber, installed perpendicular in front of a reflector, and the reflecting surface itself (see Fig. 2). This setup has been realized and successfully applied in different fields of research in the past (e.g., Refs. [20,21]).

Since both interfering beams travel the fiber, vibrations changing the optical length of the fiber influence the traveled distance of both reflections and consequently no influence on the relative phase between the interfering beams occurs. In Fig. 2, L represents the length of the FP cavity. Since the difference of the two traveled distances of the two interfering beams is short ($2L$), the resulting demand on the laser light source concerning the coherence length is quite low. The reflection at the fiber end results from the interface *glass fiber—cavity*, where the change in the refractivity induces a reflection of ~4% (see, e.g., Ref. [22]).

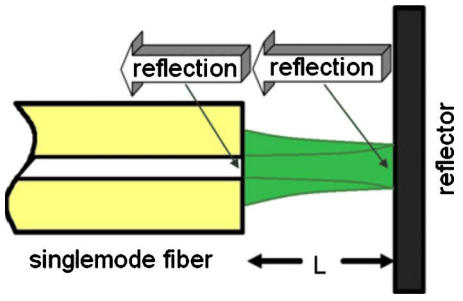

Fig. 2 Interfering reflections of a FP interferometer created between fiber end and reflector

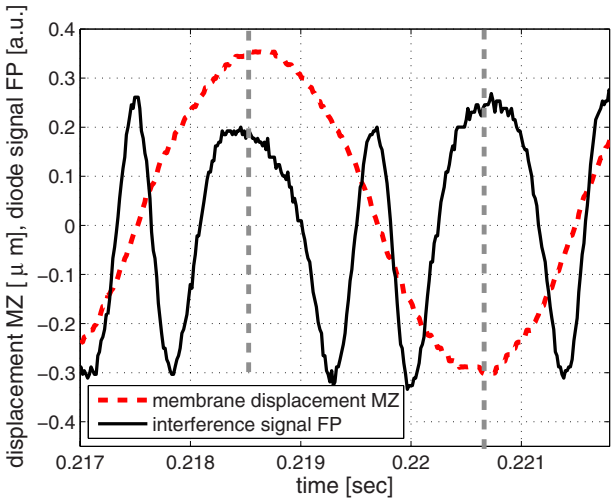

Fig. 3 A sinusoidal reflector movement measured with the FP (black solid line) and a conventional Mach–Zehnder (red dashed line) interferometer

The common projection of the two reflections on a photo receiver enables the monitoring of the resulting homodyne interference signal. An example of an interference signal is represented by the black solid line in Fig. 3 for a sinusoidal reflector movement with a frequency of 250 Hz. The corresponding original reflector movement is illustrated by the red dashed line, measured with a commercial MZ interferometer. The interference signal represents the phase dependent change between constructive and destructive interference between the two reflections. Such a change between destructive and constructive interference represents a reflector movement of one quarter of the wavelength of the laser light source used [23], i.e., in case of a green laser with a wavelength of 532 nm the change between constructive and destructive interference represents a reflector movement of 133 nm. At the extrema of the reflector movement, when the reflector changes its direction of movement, the interference signal reaches its reversal point and the signal is mirrored on a vertical line passing this reversal point, as shown schematically by the gray vertical lines in Fig. 3. These two lines indicate the distance between two consecutive extrema of the measured reflector movement. The time distance between two extrema encodes the frequency of the reflector movement, whereas the number of changes between constructive and destructive interference in such a time interval encodes the amplitude of the reflector movement. For the interpretation of such a simple homodyne interference signal, the fringe-counting method is often used (see, e.g., Ref. [24]). But the classical fringe-counting procedure, where the changes between constructive and destructive interference are counted to calculate the amplitude of the reflector movement, shows a quite limited resolution since only entire steps from constructive to destructive interference (and vice versa) can be processed. A further grading of the signal is only possible with highly stable optical signals. A signal encoding several frequencies requires special efforts for interpretation.

The exemplary test case shown in Fig. 3 already presents a quite high membrane displacement with an amplitude of about 300 nm, which can be reached in reality only with quite high pressure fluctuations. The dynamic range of an FOM using such a basic FP interferometer is not satisfactory for its application in thermo-acoustic experiments. A novel approach to enhance the resolution of the optical setup is subsequently described, which extends the dynamic range of the new sensor in comparison to sensors proposed in the past.

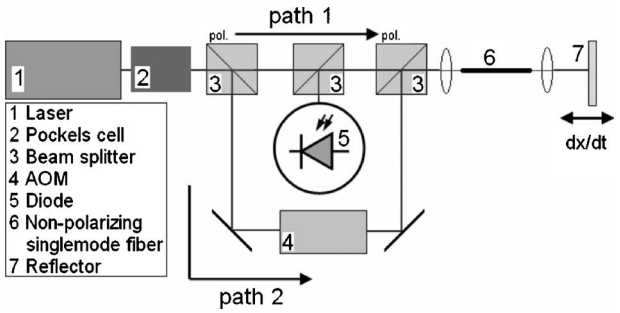

Fig. 4 Optical setup of the FOM based on a FP interferometer

3 The Advanced FP Interferometer Setup

Due to these fundamental advantages of the fiber FP interferometer, an optical setup, increasing the dynamic range of the resulting FOM, has been designed to enable the later application of the new sensor under hot conditions. This optical setup has to be placed in front of the glass fiber as shown in Fig. 4 to create two quasi simultaneously acquirable homodyne interference signals both encoding the same reflector movement and fulfilling the quadrature condition, i.e., the signals have a constant phase distance of 90 deg. Similar methods are generally called quadrature homodyne interferometry.

The designed setup extension creates two laser modes out of one laser beam, whereas for the aspired kind of signal generation the wavelengths of the two laser modes creating two homodyne interference signals with a 90 deg phase distance have to be characterized by a constant frequency distance $\Delta\nu$ adapted to the length L of the FP cavity following Eq. (1) [25]:

$$L = \frac{\lambda/4 \cdot \nu_0}{2 \cdot \Delta\nu} = \frac{c}{8 \cdot \Delta\nu} \tag{1}$$

Here, λ represents the wavelength of the laser light used, ν_0 is the fundamental frequency of the laser light, and c is the speed of light. As Eq. (1) shows, the required distance L depends on the frequency distance between the two modes but is independent of the wavelength of the laser light used.

Different possibilities of creating similar systems are reported in literature, e.g., the use of two laser diodes [26] or the use of a multimode laser in combination with optical filters [20]. Since the aim of the presented project is the simple application of the FOM for all kind of acoustic measurements in harsh environments, the optical setup has to be realized as simple as possible, i.e., with a minimum amount of optical components and one laser light source only.

Figure 4 shows schematically the arrangement of the designed optical setup, which is mainly based on the use of an optical switch, realized with a Pockels-cell (2), and an acousto-optical modulator (AOM) (4) to create the constant frequency distance $\Delta\nu$ between the two laser beams. The optical setup presented in the following contains a laser light source (1) with a nominal optical power of 200 mW and a wavelength of 532 nm. The laser beam is switched by means of the mentioned Pockels-cell (2) between the two in Fig. 4 indicated optical paths, whereas both, feeding the fiber based FP interferometer, create homodyne interference signals on the photodiode (5). Path 2 includes the AOM in order to create the constant frequency distance $\Delta\nu$.

To get a cavity length L acceptable for the design of an acoustical sensor head, an AOM with a frequency shift of 540 MHz has been chosen. Thus, a cavity length L of $\sim$70 mm has to be used in the sensor head design to obtain the constant 90 deg phase difference between the two interference signals. Since the optical switch activates the two paths alternately according to the control signal of the cell, the two interference signals are not acquired simultaneously. A high switching frequency of the cell, however, enables the correct reconstruction of the two homodyne interference signals by means of averaging and linear interpolation, thus, the signals are acquired quasi simultaneously.

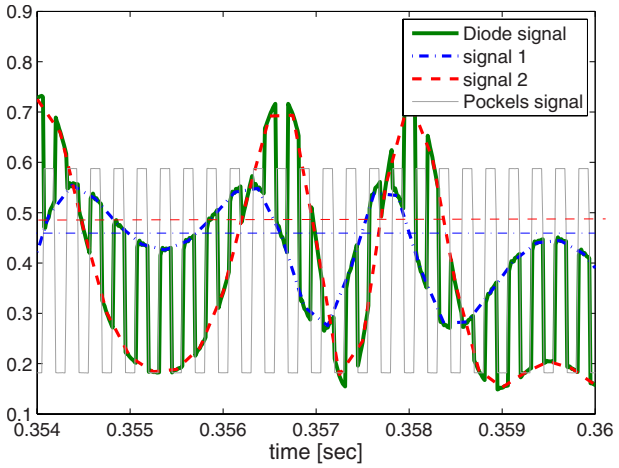

Fig. 5 Single-frequency-excitation: acquired signals of the advanced FP setup

Figure 5 presents an example of the acquired time signals for a one frequency movement of the reflector: the diode signal (green solid line) and the Pockels-cell control signal (gray thin solid line), which has to be used to separate the two interference signals (unequally dashed lines), which appear as the envelopes of the diode signal. Further processing of data to obtain the original reflector movement is done using the arc tangent function of the quotient of the two separated interference signals. Due to their constant 90 deg phase distance the polar diagram of the two signals represents a constant circle. Figure 6 shows the case of a sinusoidal reflector movement: The upper left shows the two separated homodyne interference signals (black solid and green dashed line, respectively), the right the corresponding polar diagram. The pointer (red) added in the polar diagram presents the vector to the signal pair of the two separated homodyne interference signals; its movement can be interpreted to get the original membrane movement.

- The rotational speed of the pointer represents the velocity of the reflector movement.
- The change in the direction of rotation represents the change in the direction of movement of the reflector.

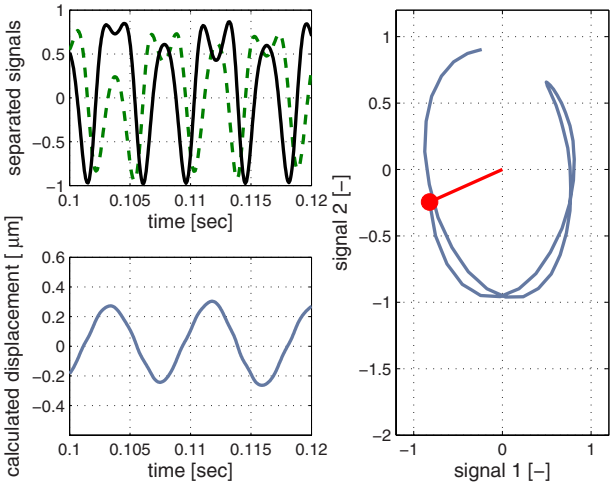

Fig. 6 Signal processing for the advanced FP setup

Fig. 7 FOM sensor head—photograph

- A closed circle in the polar diagram represents a reflector movement of half the wavelength of the laser light used.

This information leads to the original reflector movement (blue) as shown in the lower left in Fig. 6.

To realize an FOM based on this optical setup, a sensor head, connecting the membrane with the fiber, has been manufactured. Figures 7 and 8 show a photograph and a technical drawing of the 70 mm long FOM sensor head, respectively. The diameter of the active area of the membrane is 6 mm. In the technical drawing, the positions of membrane, lens and fiber end are indicated. Aluminum foils and stainless steel foils (thickness of the foils: varied between 5 μm and 50 μm) were studied for membrane materials. Due to the dependence of the membrane stiffness on the Young's modulus of the membrane material and on the membrane thickness, the sensitivity of the sensor can be varied according to the desired case of application by varying its membrane properties. The membranes were clamped on the hollow cylinder with a retaining ring. Thus, they were very easily and inexpensively replaceable and offer a handling, which is much easier for the designed FOM than for conventional condenser microphones. The position of the membrane regarding the fiber end is adjustable by screwing the sensor head on the lens containing connecter.

4 Experimental Results: Acoustic Measurements With the FOM

The presented results were all obtained with stainless steel membranes since this type of membrane material has to be employed for the application at elevated temperature levels.

4.1 Results Obtained With the FP Setup Under Cold Conditions: Sweep Excitation and Multitone Excitation. The FOM was calibrated by means of a pistonphone to determine the sensor sensitivity. Depending on the thickness of the used stainless steel membrane diverse sensitivities could be reached. With a stainless steel membrane, thickness 12.5 μm, the resulting sensor sensitivity was $\sim$20 nm/Pa. Membranes with a thickness of $\sim$20 μm resulted in sensitivities of $\sim$6 nm/Pa.

The calibrated sensor was then applied in a square cold acoustic test rig to study its performance measuring different acoustic excitation states. The acoustic driver was a loudspeaker. As reference sensor a conventional condenser microphone was placed in

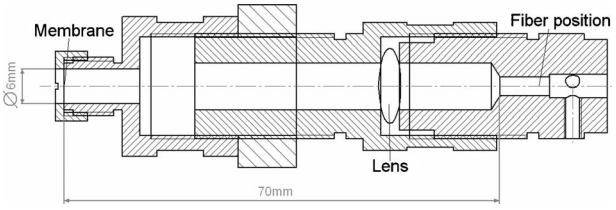

Fig. 8 FOM sensor head—technical drawing

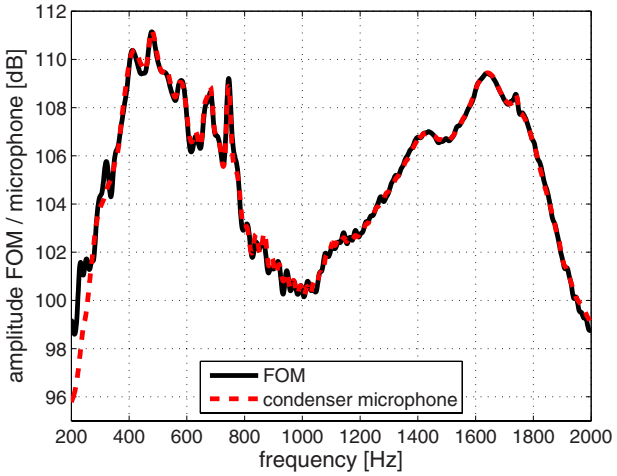

Fig. 9 Spectra of FOM and condenser microphone for sweep excitation between 200 Hz and 2000 Hz

parallel at the same axial position as the FOM was installed with an azimuthal displacement of 90 deg. Thus, the transfer function of the two calibrated sensors has theoretically a constant amplitude of 1 and a constant phase of 0. The test section was connected to an anechoic termination to minimize acoustic reflections.

The first excitation test case was a frequency sweep from 200 Hz to 2000 Hz. Figure 9 presents the two spectra of the two sensor types, whereas the sound pressure level was calculated with the reference 2×10^{-5} Pa. The spectrum of the FOM is represented by the black solid line, the spectrum of the conventional condenser microphone by the red dashed line. Due to the fact that both sensors were calibrated, the spectra show the sound pressure level versus the frequency. The comparison of both spectra demonstrates a very high agreement and confirms the good performance of the new sensor for similar applications. Figure 10 shows the coherence between the two signals and attests the noticed agreement of the sensor signals. Figures 11 and 12 present the transfer function of the two sensors, i.e., the amplitude, which is close to the theoretically assumed value of 1, and the phase, which is close to 0. Since the frequency range of excitation lies below the first cut-on frequency of the acoustic duct ($\sim$2143 Hz), no influence of sound waves propagating in higher modes has to be

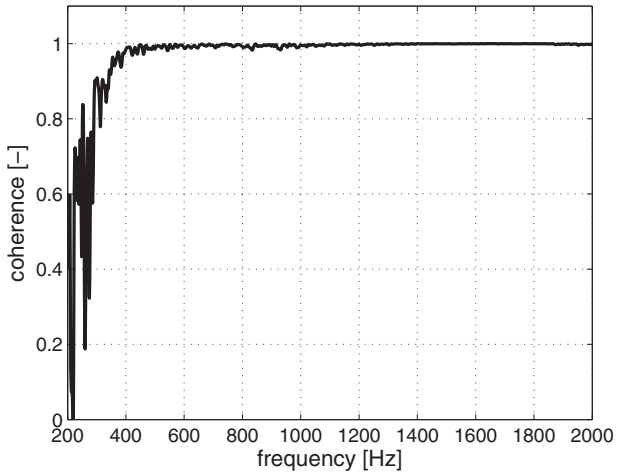

Fig. 10 Coherence between the sensors for sweep excitation between 200 Hz and 2000 Hz

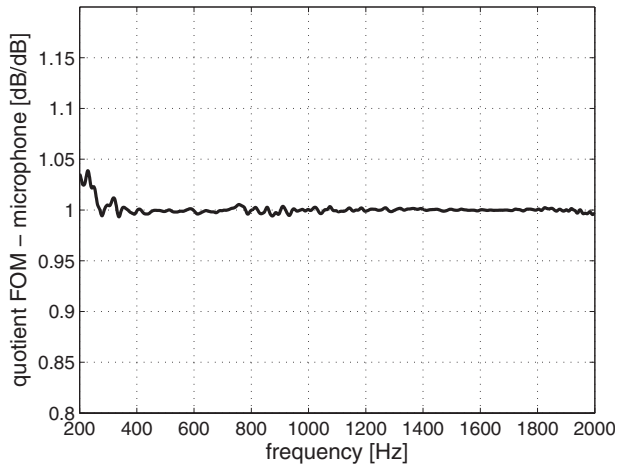

Fig. 11 Transfer function for sweep excitation: amplitude

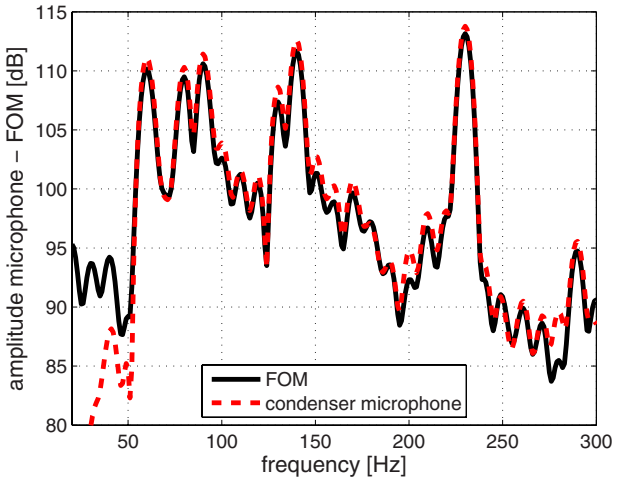

Fig. 13 Spectra of FOM and condenser microphone for low-frequency multitone excitation

considered.

In a second test case an acoustic excitation was chosen, which is more relevant for thermo-acoustic studies than a sweep excitation: the multitone excitation in the frequency range below 300 Hz. For this purpose, several frequencies between 60 Hz and 250 Hz were excited simultaneously. The black solid line in Fig. 13 represents the spectrum of the FOM signal, the red dashed line the spectrum of the acquired condenser microphone signal. The high agreement between the spectra of the FOM and the condenser microphone shows both the stability of the optical signal and the stability of the data processing procedure, and finally the later applicability of the new sensor for thermo-acoustic studies.

4.2 Application Under Hot Conditions: Installation in an Atmospheric Combustion Chamber. As a first test under hot conditions, the FOM was applied in an atmospheric combustion chamber, which was operated at a thermal power of ~8.4 kW at stoichiometric combustion conditions with an exhaust gas temperature of ~1000 K at the combustor outlet. To enable the comparison of the FOM result to an established measurement technique for research applications at elevated temperature levels, a probe sensor based on a conventional condenser microphone was installed in parallel in the combustion chamber. The design of the probe sensor used is shown in Fig. 14. This design of the German Aerospace Centre (DLR e.V.) uses a semi-infinite tubing to guide the acoustic wave to the microphone placed perpendicular to the tubing. This tubing has to be flushed with air to avoid the inflow of exhaust gas into the tube affecting the sensitivity of the microphone membrane. Due to the transfer function of this tubing, the signal of the condenser microphone has to be corrected in post-processing to get the data of a theoretically wall flush-mounted sensor [12].

More details about the combustion chamber and its analysis regarding combustion oscillations can be found in Refs. [13,14]. The combustion chamber wall made of stainless steel was permanently at red heat. Figure 15 presents on the right a photograph of the combustion test rig driven at the studied test case. The left side shows the accordant three-dimensional design drawing of the combustion chamber and the installed acoustic sensors. A principle top view is displayed in Fig. 16 to clarify the location of the sensors: The FOM was placed at the same axial position as one of the two installed probe sensors but with an azimuthal displacement of 90 deg. The FOM head was wall flush-mounted installed and, thus, its membrane was directly exposed to flue gases and flame radiation. Due to the low mass of the membrane, it can be assumed that the sensor head temperature lies in the range of the gas temperature measured at the combustor outlet.

Figure 17 illustrates the spectra of the two sensor signals for the studied operating point. The spectrum of the probe microphone (red dashed line) shows the sound pressure level, the spectrum of

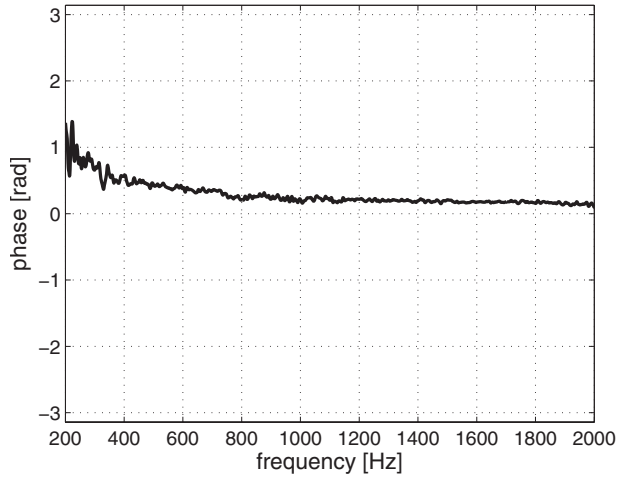

Fig. 12 Transfer function for sweep excitation: phase

Fig. 14 DLR in-house design probe microphone

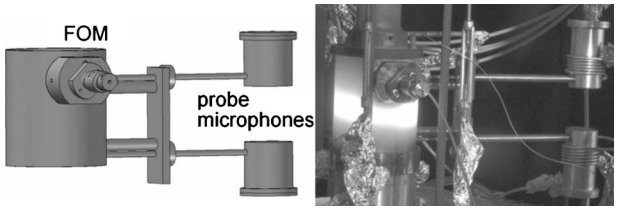

Fig. 15 Combustion chamber: design drawing of flame tube (L) and photograph (R)

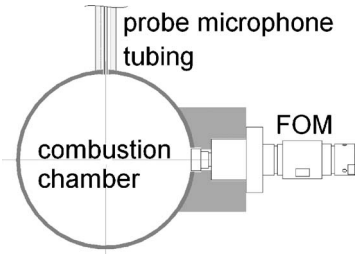

Fig. 16 Schematic top view of the combustion chamber

the FOM (black solid line), and the measured membrane displacement. The peak at ~85 Hz in both spectra represents the thermoacoustic instability of the analyzed operating point of the combustion test rig. The high agreement between the two spectra shows again the applicability of the designed sensor for combustion diagnostic measurements. The applied sensor head was based on a stainless steel membrane with a thickness of 20 μm. The low membrane displacement at relatively high acoustic sound pressure levels (less than 1 μm at 153.5 dB) shows a decreased sensor sensitivity (<1 nm/Pa) at this increased application temperature. This observation, however, was not expected a priori and its occurrence is still under investigation. One possible explanation is the occurrence of an increased membrane tension due to thermally caused deformation of the sensor head.

5 Potential Sensor Improvements

The performance of the designed sensor depends highly on the performance of the optical components used. As Fig. 5 clarifies, the switching frequency between the two optical paths has to ensure a correct separation of both interference signals. The higher the acoustic frequency is, the higher the Pockels-cell switching frequency must be to get the full information of both paths. Also, a higher amplitude requires a higher switching frequency since the amplitude influences the amount of changes between constructive and destructive interference. A switching frequency too low for the correct separation of the two interference signals leads to a loss of information and, thus, the correct membrane movement is not reconstructible.

Figures 18–20 represent this circumstance: a high switching frequency enables the reconstruction of both interference signals at high quality; with decreasing switching frequency, however, the reconstructed interference signals lose their smooth shape and, thus, necessary information for a high-quality analysis of the accordant polar diagram gets lost. This fact is visible in the polar

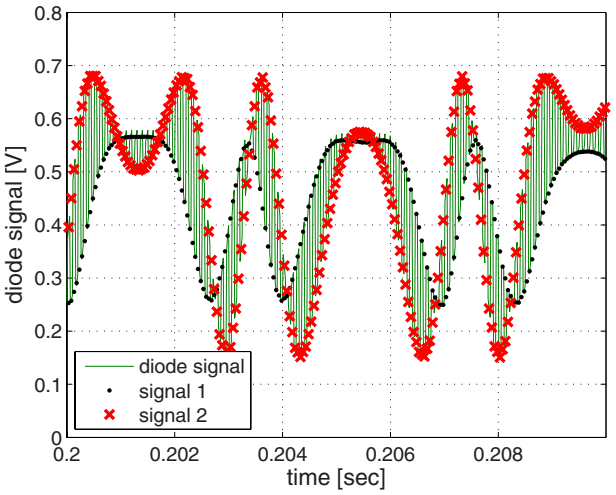

Fig. 18 Pockels-cell switching frequency high (10 kHz)

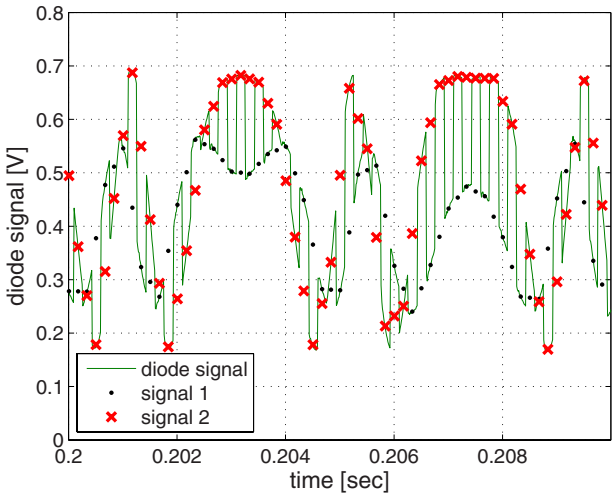

Fig. 19 Pockels-cell switching frequency low (3 kHz)

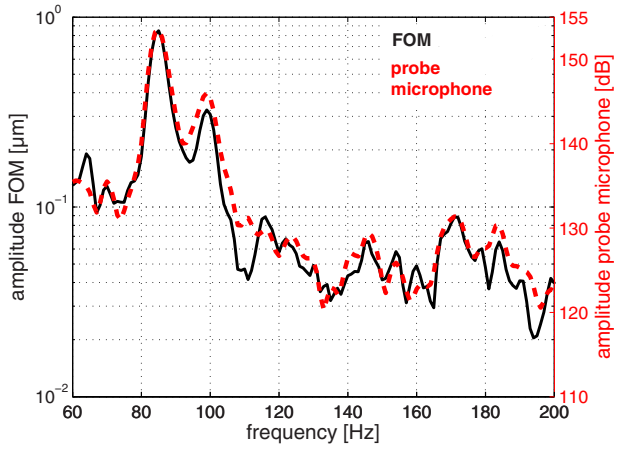

Fig. 17 Spectra FOM and probe microphone applied in a combustion chamber

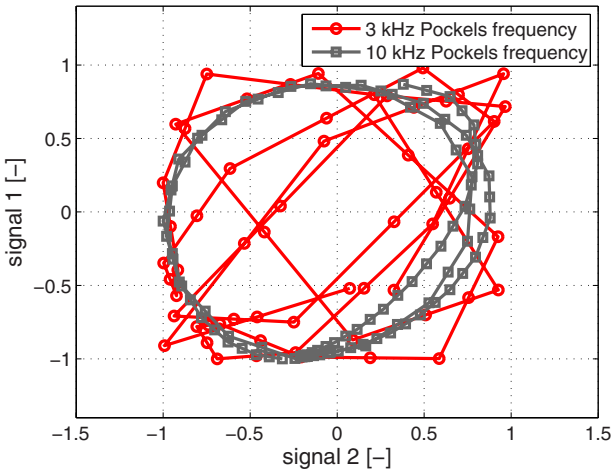

Fig. 20 Polar diagram: variation of the Pockels-cell switching frequency from 3 Hz to 10 kHz

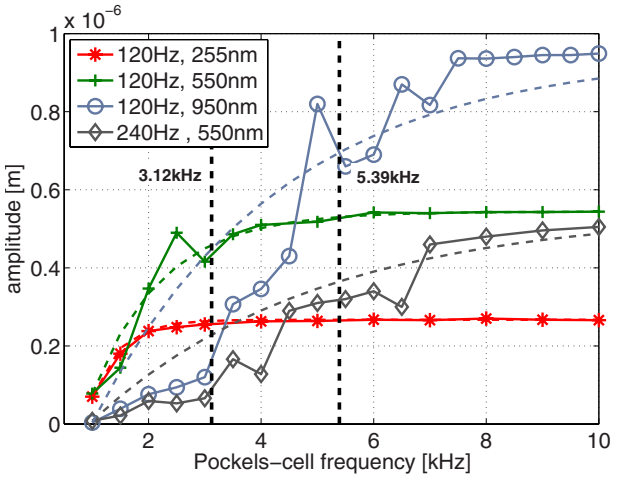

Fig. 21 Required Pockels-cell switching frequency—comparison experiment and theory

diagram since the common representation of the reconstructed interference signals is not circular anymore. Figure 20 shows an example, where the Pockels-cell switching frequency was decreased from 10 kHz to 3 kHz. From the theoretical point of view, a minimum Pockels-cell switching frequency, needed to ensure the correct reproduction of the membrane movement, is declarable by the demand of phase distances of less than *pi* between successive samples. Thus, for a fixed amplitude A of object movement, a minimum sampling frequency f_s can be calculated accordant to Eq. (2) (see, e.g., Refs. [27,28]),

$$f_s = 4 \cdot A \cdot \frac{2\pi}{\lambda} \cdot f \tag{2}$$

where f represents the frequency of object movement and λ represents the optical wavelength of the laser light used.

This fact has also been studied experimentally by measuring the movement of membranes, excited at different acoustic frequencies and with different amplitudes of membrane movement, whereas the switching frequencies of the Pockels-cell were varied. The reconstructed time signals of the membrane movements were Fourier transformed and the amplitudes were plotted versus the Pockels frequency. Figure 21 shows the result of this study: since the excitation case was kept constant for each experimental series, the real amplitude of the membrane movement is constant as well; a Pockels-cell frequency, however, which does not allow the correct recalculation of the membrane movement, results in an amplitude that lies below this real value. As Fig. 21 clarifies, the minimum Pockels-cell switching frequency is reached when the asymptotic value of the calculated amplitudes is reached. The mentioned theory applied for the test case with a frequency of 120 Hz and an amplitude of ~550 nm of the object movement leads to a minimum Pockels-cell switching frequency of ~3.12 kHz (indicated in Fig. 21 by the left vertical, dashed line). This value fits approximately the experimental result, i.e., the frequency needed to reach the asymptotic threshold of the amplitude. The test case of 120 Hz and ~950 nm amplitude, however, shows that theory and experiment deviate from each other, the experiment seems to require much higher switching frequencies (the right vertical, dashed line indicates the theoretically required Pockels-cell frequency). This may result from the stability of the optical signal in the experiment and the stability of the data processing routine. For the experimental use of the sensor, the Pockels-cell switching frequency has to be chosen as high as possible to broaden the applicability of the sensor regarding both frequency and dynamic range.

Since a Pockels-cell requires a high voltage control signal, its performance at square wave control signals required for the presented application, suffers at frequencies in the range of 10 s of kHz. An improvement can be the substitution of the Pockels-cell with an other optical switch that requires less effort for a high-quality switching behavior, e.g., the combination of two AOMs. This approach also gives the possibility of using the frequency shift coming from the optical switch to create the frequency distance $\Delta\nu$ between the two required laser modes.

6 Conclusion

The way to build a high temperature resistant fiber-optical microphone applicable for acoustic measurements under hot conditions and its successful application was presented. With a first prototype a direct measurement of combustion oscillations without the requirement of special cooling devices was effectively performed in a combustion chamber at a thermal power of ~8.4 kW and a gas temperature of ~1000 K in the vicinity of the sensor head.

The core of the designed optical sensor is a fiber Fabry–Perot interferometer. The optic setup is designed to reach a resolution that allows the detection of acoustically induced membrane displacements. Therefore, the sensor creates quasi simultaneously two homodyne interference signals, which fulfill the quadrature condition and can be evaluated to calculate the membrane movements. Detailed experiments under cold conditions confirmed the high-quality performance of both the optical setup and the data processing procedure.

The proposed sensor will help to solve the problems of the state-of-the-art measurement techniques for combustion driven pressure oscillations regarding cooling and data processing.

Acknowledgment

We acknowledge dedicated support from our student coworkers Alexandre Buffet, Andrea Gärtlein, Joshua Gray, and Mirko Spitalny. Furthermore, we thank André Fischer and Karsten Knobloch for their support during the measurements at the combustion test rig. Finally, we thank the Helmholtz Association for the financial support in the framework of the Helmholtz-University Young Investigators Group New Optical Measurement Techniques for Turbomachinery Diagnostics.

Nomenclature

A = amplitude of object movement
c = speed of light
f = frequency of object movement
f_s = minimum switching frequency of Pockels-cell
L = length of the Fabry–Perot cavity
λ = wavelength of the laser
ν_0 = frequency of the laser light
$\Delta\nu$ = frequency shift created by the Acousto-Optical Modulator

References

[1] Paschereit, C. O., Schuermans, B., Polifke, W., and Mattson, O., 2002, "Measurement of Transfer Matrices and Source Terms of Premixed Flames," ASME J. Eng. Gas Turbines Power, **124**, pp. 239–247.
[2] Lubarsky, E., Shcherbik, D., Bibik, A., and Zinn, B. T., 2003, "Active Control of Combustion Oscillations by Non-Coherent Fuel Flow Modulation," Ninth AIAA/CEAS Aeroacoustics Conference and Exhibit, South Carolina, Paper No. AIAA 2003-3180.
[3] Guyot, D., and Paschereit, C. O., 2007, "Active Control of Combustion Instability Using Symmetric and Asymmetric Premix Fuel Modulation," ASME Paper No. GT2007-27342.
[4] Bothien, M. R., 2008, "Impedance Tuning: A Method for Active Control of the Acoustic Boundary Conditions of Combustion Test Rigs," Ph.D. thesis, TU Berlin.
[5] Schuermans, B., Guethe, F., and Mohr, W., 2008, "Optical Transfer Function Measurements for Technically Premixed Flames," ASME Paper No. GT2008-51500.
[6] Alemela, P. R., Fanaca, D., Ettner, F., Hirsch, C., and Sattelmayer, T., 2008, "Flame Transfer Matrices of a Premixed Flame and a Global Check With Modelling and Experiments," ASME Paper No. GT2008-50111.

[7] Broukaert, J.-F., Mersinligil, M., and Pau, M., 2008, "A Conceptual Design Study for a New High Temperature Fast Response Cooled Total Pressure Probe," ASME Paper No. GT2008-51054.
[8] Ferrara, G., Ferrari, L., and Sonni, G., 2005, "Experimental Characterization of a Remoting System for Dynamic Pressure Sensors," ASME Paper No. GT2005-68733.
[9] Fernandes, E. C., 2005, "The Design of Sound Probes," Twelfth International Congress on Sound and Vibration, Portugal.
[10] Wegner, M. A., Nance, D., and Ahuja, K. K., 2007, "Characterization of Short and Infinite-Line Pressure Probes for In-Duct Acoustic Measurements Under Hostile Environment," Thirteenth AIAA/CEAS Aeroacoustics Conference, Italy, Paper No. AIAA 2007-3443.
[11] Diers, O., Schneider, D., Voges, M., Weigand, P., and Hassa, C., 2007, "Investigation of Combustion Oscillations in a Lean Gas Turbine Model Combustor," ASME Paper No. GT2007-27360.
[12] Fischer, A., Bake, F., and Röhle, I., 2008, "Broadband Entropy Noise Phenomena in a Gas Turbine Combustor," ASME Paper No. GT2008-50263.
[13] Bake, F., Michel, U., and Röhle, I., 2007, "Investigation of Entropy Noise in Aero-Engine Combustors," ASME J. Eng. Gas Turbines Power, **129**(2), pp. 370–376.
[14] Bake, F., Kings, N., Fischer, A., and Röhle, I., 2009, "Experimental Investigation of the Entropy Noise Mechanism in Aero-Engines," Int. J. Aeroacoust., **8**(1–2), pp. 125–142.
[15] Bake, F., Kings, N., Fischer, A., and Röhle, I., 2009, "Indirect Combustion Noise: Investigations of Noise Generated by the Acceleration of Flow Inhomogeneities," Acta. Acust. Acust., **95**(3), pp. 461–469.
[16] Bake, F., Fischer, A., Kings, N., and Röhle, I., 2009, "Investigation of the Correlation of Entropy Waves and Acoustic Emission in Combustion Chambers," *Combustion Noise*, A. Schwarz and J. Janicka, eds., Springer, Heidelberg, Berlin, pp. 125–146.
[17] Parrott, T. L., and Zorumski, W. E., 1992, "Sound Transmission Through a High-Temperature Acoustic Probe Tube," AIAA J., **30**(2), pp. 318–323.
[18] Konle, H. J., Spitalny, M., Paschereit, C. O., and Roehle, I., 2009, "Design and Application of Fiber-Optic Microphones for Thermo-Acoustic Measurements," Fifth AIAA/CEAS Aeroacoustics Conference (30th AIAA Aeroacoustics Conference), Paper No. AIAA 2009-3300.
[19] Konle, H. J., Rausch, A., Fischer, A., Doll, U., Willert, C. E., Paschereit, C. O., and Röhle, I., 2009, "Development of Optical Measurement Techniques for Thermo-Acoustic Diagnostics: Fibre-Optic Microphone, Rayleigh-Scattering, and Acoustic PIV," International Journal of Spray and Combustion Dynamics, **1**(2), pp. 251–281.
[20] Fürstenau, N., Schmidt, M., Horack, H., Götze, W., and Schmidt, W., 1997, "Extrinsic Fabry–Perot Interferometer Vibration and Acoustic Sensor Systems for Airport Ground Traffic Monitoring," IEE Proc.: Optoelectron., **144**(3), pp. 134–144.
[21] MacPherson, W. N., Kilpatrick, J. M., Barton, J. S., and Jones, J. D. C., 1999, "Miniature Fiber Optic Pressure Sensor for Turbomachinery Applications," Rev. Sci. Instrum., **70**(3), pp. 1868–1874.
[22] Davis, P. G., Bush, I. J., and Maurer, G. S., 1998, "Fiber Optic Displacement Sensor," Proceedings of SPIE, Fourth Pacific Northwest Fiber Optic Sensor Workshop, May 6, Vol. 3489.
[23] Jackson, D. A., 1985, "Monomode Optical Fibre Interferometers for Precision Measurement," J. Phys. E, **18**, pp. 981–1001.
[24] Tomita, E., and Kawahara, N., 2008, "Temperature Measurement of Water With Sensor by Laser Interferometry Technique," Fourteenth International Symposium on Application of Laser Techniques to Fluid Mechanics, Portugal.
[25] Ezbiri, A., 1995, "Passive Signal Processing for a Miniature Fabry–Perot Interferometric Sensor With a Multimode Laser-Diode Source," Opt. Lett., **20**(17), pp. 1818–1820.
[26] Wright, O. B., 1991, "Stabilized Dual-Wavelength Fiber-Optic Interferometer for Vibration Measurement," Opt. Lett., **16**(1), pp. 56–58.
[27] Cranch, G. A., and Nash, P. J., 2001, "Large-Scale Multiplexing of Interferometric Fiber-Optic Sensors Using TDM and DWDM," J. Lightwave Technol., **19**(5), pp. 687–699.
[28] Kirkendall, C. K., and Dandrige, A., 2004, "Overview of High Performance Fiber-Optic Sensing," J. Phys. D, **37**, pp. R197–R216.